On topological Properties of Superconducting Nanowires

Pikulin, D.

Chapter 1

Introduction

1.1 Preface

There are many concepts in quantum mechanics that are counter-intuitive from the everyday life perspective. They range from the Heisenberg uncertainty principle to the concept of entangled states. Recently the collection has been enriched by the topological states of matter. They have intrinsic "skin effect", so that all the particle current flows on their surface, while the bulk of the material is insulating. This property does not depend on the exact details of a sample, disorder, etc. This is the reason the states are called topological. The first example of such states is the 2d Quantum Hall effect [1]. Later ones are Quantum Spin Hall [2–4] effect, 3d Topological Insulators [5–7] and Topological Superconductors [8, 9]. The results of the first experiments observing Quantum Hall and Spin Hall effects are in fig. 1.1. All the effects can be described in the framework of non-interacting quasiparticles above the Fermi sea. Based on this observation, the general classification of such topological states is constructed [10].

The most vivid example of the counter-intuitive structure of such materials is the Majorana fermion, which emerges on the boundary of a topological superconductor [11, 12] or in half-integer vortices in the topological superconductors [13, 14]. Majorana fermion is neither an electron nor a hole (absence of electron), it is half-electron half-hole at the same time. No classical analogy helps to understand this quasiparticle, as a half-empty glass is not an empty and a filled glass simultaneously. It is not a state that is empty in half of the cases and filled in

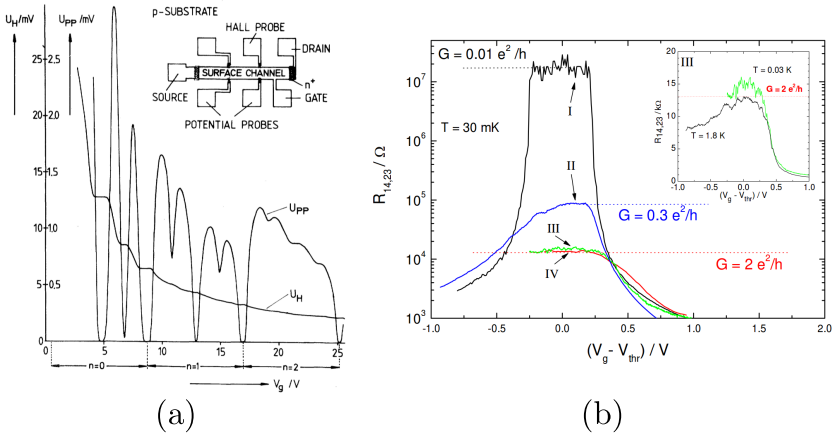

Figure 1.1. First measurements of the two topological systems in 2 dimensions. (a) Quantum Hall effect [1] conductance measurement as a function of gate voltage. The gate tunes through the plateaus for the Hall voltage (U_H) and dips in the voltage along the device (U_{PP}). (b) Quantum Spin Hall effect [4] conductance measurement as a function of gate voltage, tuning through the bandstructure of the material and showing quantized conductance in the bulk gap. Reprinted with permission from AAAS.

the other half. Rather it can be understood literally as a state, which is half of an electron and half of a hole at the same time. Only by bringing it together with another Majorana, it can really be measured if the combination of them is a full electron or a full hole. This property protects the state from any kind of local potential perturbation and makes devices based on it good candidates for a quantum memory [15] and quantum computations [16–18]. The name "Majorana fermion" comes from high-energy physics, where it refers to a freely moving elementary particle. In the superconducting context the Majorana is bound at zero energy to some defect (vortex or boundary), and is more precisely called "Majorana bound state" or "Majorana zero-mode". The combined object (Majorana plus defect) is actually not a fermion but a more exotic object called a "non-Abelian anyon" [19].

Majorana fermions are predicted to emerge on the boundary of both 1d and 2d topological superconductors [9, 10, 20–22]. They can be either propagating or localized excitations. As the title of the present thesis suggests, we deal with the 1d examples, which are bound states, in the setups of realistic quantum wires. The Majorana bound states are pre-

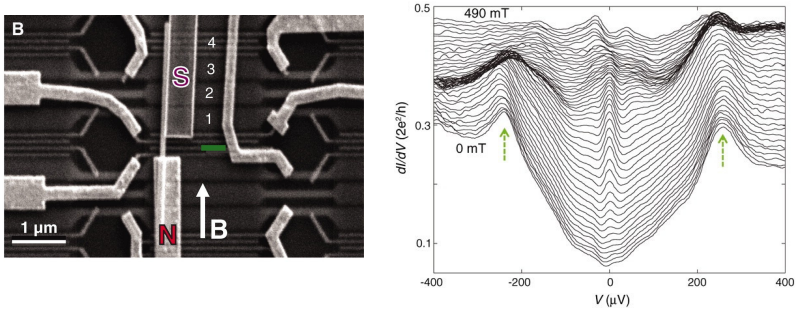

Figure 1.2. The first measurement of conductance for a spin-orbit coupled nanowire (setup on the left), showing zero-bias conductance peak, taken from [23]. The setup is very similar to the one we study in the chapter 4. Reprinted with permission from AAAS.

dicted to emerge in spin-orbit coupled nanowires under external magnetic field and in contact with the usual s-wave superconductors [21, 22]. Recently the predictions have found supporting experimental evidence [23–26]. Measurement from [23] is shown in fig. 1.2.

We start by examining the topological transition in finite wires and show that though it becomes a crossover there is a transition of different kind, which stays sharp. Then using model-independent techniques we study the wires in the vicinity of the two transitions, where their properties become universal. We study the effect of disorder in the nanowires also in a model-independent way. Then we discuss Josephson junctions with Majorana bound states of different lengths and in different setups: voltage biased short junction and phase biased long junction. We finish with a detour into the theory of Nernst effect in materials with anisotropic scattering and Fermi-surfaces.

1.2 Majorana bound state

Let us introduce the notion of the Andreev bound state. It is a state, which is localized in the vicinity of the superconductor and the wavefunction of which has both electron and hole component. Majorana bound state is a particular type of the Andreev bound state, when the

electron and hole component have equal weights:

$$\gamma_1 = \psi + \psi^\dagger, \tag{1.1}$$

$$\gamma_2 = i(\psi - \psi^\dagger), \tag{1.2}$$

where ψ is the electron annihilation operator and γ is the Majorana operator:

$$\gamma = \gamma^\dagger. \tag{1.3}$$

Particle-hole symmetry in the superconductors connects the creation and annihilation operators at energies $\pm E$ counted from the middle of the superconducting gap and requires:

$$\gamma(E) = \gamma^\dagger(-E), \tag{1.4}$$

therefore Majorana bound state can only appear at zero energy, in the middle of the gap.

1.2.1 Systems for observing Majorana bound state

In this thesis we will study two systems, where the Majorana bound state may emerge: the edge of the Quantum Spin Hall insulator and the spin-orbit nanowire in an external magnetic field, both coupled by proximity effect to the usual s-wave superconductor.

For the purposes of the present thesis it is important to know that the Quantum Spin Hall insulator can be thought of as two copies of the Quantum Hall systems with opposite magnetic fields, so that they are time-reversal partners of each other. This means that the Quantum Spin Hall system also has insulating bulk, but two copies of the Quantum Hall chiral edges. They are going in the opposite directions and are forming a Kramers pair. The latter forbids the scattering from one state to counter-propagating if the time-reversal symmetry is preserved. The dispersion of one edge of the Quantum Spin Hall insulator is shown in fig. 1.3.

Superconductor in proximity with the Quantum Spin Hall edge opens the gap in the edge dispersion, but the argument above still holds and it is forbidden to scatter from the right-moving to the left-moving state of an electron. Nevertheless, the superconductor opens up another possibility for backscattering: Andreev reflection [27]. It is the process of

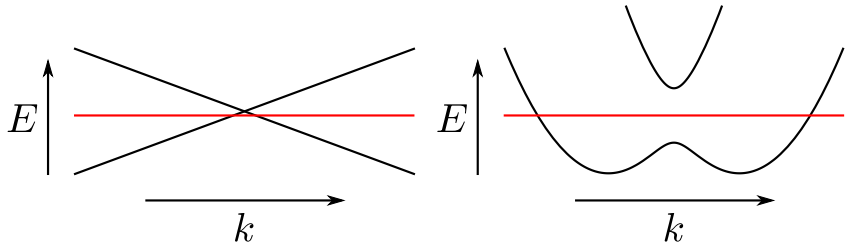

Figure 1.3. Schematic depiction of the dispersion relation of the edge states of the Quantum Spin Hall insulator (left) and the lowest band of the single-channel spin-orbit nanowire (right), the two materials being used for the detection of the Majorana fermions. The Fermi level is shown with the horizontal red line

an incident electron reflecting back as a hole and transferring a Cooper pair into the superconductor. As described above, the normal reflection is forbidden in the Quantum Spin Hall system and there is an ideal Andreev reflection. It turns out that if one breaks time-reversal symmetry, the ideal Andreev reflection is lost except at zero bias. The zero-bias peak in Andreev conductance is one of the signatures of Majorana bound state [28, 29]. It is clear that the Andreev bound state near the normal metal-superconductor boundary in such a system will have the Majorana nature, as the Andreev reflection is perfect, the wavefunction of the state is forced to be equally electron- and hole-like. Schematically the arrangement is shown in fig. 1.4.

What is the similarity between the Quantum Spin Hall edge and the spin-orbit nanowire, the other setup we discuss in the thesis? It turns out that the crucial factor for the Majoranas to emerge is the non-degenerate conducting channel, which is obviously the case for the Quantum Spin Hall system. For the nanowire one needs quite strong spin-orbit coupling in combination with the external magnetic field to completely lift the degeneracy [21, 22]. Sketch of the dispersion relation is shown in fig. 1.3. In the nanowires one also expects to observe the Majorana-related zero-bias peak, first measurements have been reported [23–25].

The analysis of the conductance properties of the non-interacting normal-superconductor junctions is very convenient to perform with the scattering matrix formalism. Scattering matrices are powerful tools for describing the non-interacting systems [30]. Once we know the scattering matrix of the system, we can understand the conductance of it

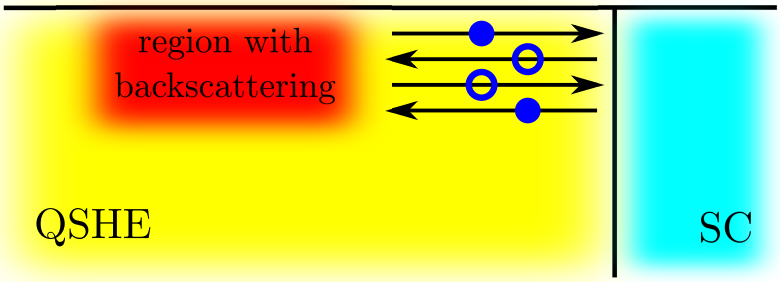

Figure 1.4. Majorana bound state formation on the edge of the Quantum Spin Hall insulator in between the region of backscattering, where time-reversal symmetry is broken, and the superconductor, which provides the Andreev reflection

both in usual and superconducting cases [31] and we apply them for the latter in the present thesis. The conductance from normal lead to the superconductor via the Andreev process is calculated as:

$$G = \frac{2e^2}{h} \mathrm{Tr}\, r_A r_A^\dagger, \tag{1.5}$$

where r_A is the subblock of the scattering matrix, corresponding to the Andreev reflection. Majorana resonant Andreev reflection manifests itself in the eigenvalue 1 of the reflection matrix at zero energy. In this thesis we will analyse the general topological properties of the scattering matrix and will use the random scattering matrix to model disordered normal-superconductor junction.

1.2.2 4π Josephson effect

Josephson effect is the phenomenon of current going between the two superconductors connected by a piece of normal metal [32]. The current may flow without resistivity if it is not too large, or if one applies voltage to the junction between the superconductors, the current is modulated with Josephson frequency [33].

Majorana bound states when present in the Josephson junction, i.e. when the weak link in the junction is the spin-orbit wire or the Quantum Spin Hall edge, has a peculiar quasi-equilibrium property: the dependence of the energy of the ground state of the junction is 4π periodic in

the superconducting phase difference between the sides of the junction [15]. By quasi-equilibrium we mean that the measurement is done faster than the parity relaxation time, or inverse tunnelling rate through one of the superconducting contacts. This is true in the current- or phase-biased case, which are discussed in the chapter 6. In the voltage-biased case, however small the tunnelling is, it affects the periodicity of the modulated current, which is discussed in the chapter 5.

The current through the Josephson junction can be calculated using the scattering matrix approach in two ways: one can derive from the scattering matrix the phenomenological Hamiltonian of the junction and study its dynamics (see chapter 5), or use the scattering matrix directly to obtain the density of states in the junction and therefore the free energy (see chapter 6). In either case it is used that the charge and superconducting phase difference are the conjugate variables and the current I can be expressed as:

$$I = \frac{2e}{\hbar}\frac{\partial F}{\partial \phi}, \tag{1.6}$$

where F is the free energy of the junction and ϕ is the superconducting phase difference between the two leads.

1.3 Symmetries

We will turn to the general classification of the topological states to understand what is the position of the topological superconductors in the classification.

The basis of the theory of a topological insulator or a superconductor is the symmetry it obeys [10]. There is a range of unitary symmetries, which a Hamiltonian can have. These include crystallographic symmetries, inversion symmetry, etc. They may also influence the classification of the Topological insulators [34], but the most important symmetries are the anti-unitary ones, time-reversal and particle-hole, and their combination, chiral symmetry. Their operators read:

$$\mathcal{T} = U_T K, \tag{1.7}$$

$$\mathcal{P} = U_P K, \tag{1.8}$$

$$\mathcal{C} = U_T U_P^*, \tag{1.9}$$

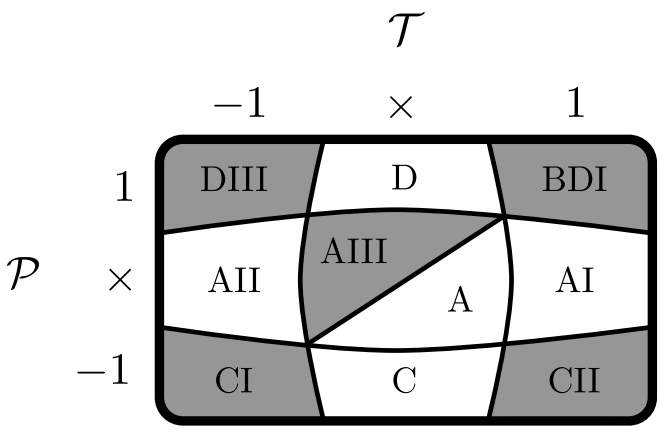

Figure 1.5. Symmetry classes of non-interacting fermions as defined by their symmetries. Numbers indicate the value of the square of the corresponding symmetry, $\times$ means the symmetry is absent. Gray areas represent symmetry classes with chiral symmetry.

where U_T and U_P are basis-dependent unitary hermitian matrices.

Though the particle-hole and the time-reversal symmetries look the same in the previous equation, they are separated by their action on the Hamiltonian:

$$\mathcal{T}H\mathcal{T}^{-1} = H, \tag{1.10}$$

$$\mathcal{P}H\mathcal{P}^{-1} = -H, \tag{1.11}$$

$$\mathcal{C}H\mathcal{C}^{-1} = -H. \tag{1.12}$$

If the symmetry is present for a system, further classification is based on the value of the $\mathcal{T}^2$ ($U_T U_T^*$) and $\mathcal{P}^2$ ($U_P U_P^*$), both can be ± 1. The simple way to see the difference between the two cases is to notice that not any Hamiltonian may be brought to the basis, where the time-reversal or particle-hole is purely complex conjugation just by rotating it with $\sqrt{U_T}$ or $\sqrt{U_P}$ correspondingly, only the ones that square to $+1$.

By this classification all the non-interacting fermion systems may be divided into 10 classes, see fig. 1.5. We will later on refer to them by the names in the table (D, BDI, CII, etc.).

These symmetries are usually based on the physical time-reversal symmetry ($\mathcal{P}^2 = -1$) and on the particle-hole symmetry, which originates from the structure of the mean-field equation for superconductors, Bogoliubov-de Gennes equation. For the latter $\mathcal{P}^2 = 1$ always.

Nevertheless a unitary symmetry may change the symmetry class of the Hamiltonian as well as the absence of some terms in the Hamiltonian due to different requirements. Let us give two examples of the change of the symmetry class of the Hamiltonian.

i. If the Hamiltonian has some unitary symmetry as an addition to the anti-unitary described above. For example:

$$\sigma_y H \sigma_y = H, \tag{1.13}$$

then along with time-reversal symmetry $\mathcal{T}$ it has

$$\mathcal{T}' = -U_T \sigma_y K, \tag{1.14}$$

$$\mathcal{T}^2 = -\mathcal{T}'^2. \tag{1.15}$$

This does not mean that the system has two time-reversal symmetries, but it means that one needs to write the Hamiltonian in the basis, where the unitary symmetry is diagonal and then study the symmetry class of each block. As the blocks are completely decoupled only the symmetry class of a single block plays a role for the physical properties of the system. Let us study an example:

$$\mathcal{T} = \sigma_y K, \tag{1.16}$$

$$\mathcal{T}' = K. \tag{1.17}$$

Then when we diagonalize the Hamiltonian, the first symmetry becomes inter-block symmetry and the second stays in-block, and squares to $+1$, which means that by the unitary symmetry we have moved the system from one symmetry class to another.

ii. When some terms are absent from the Hamiltonian due to the configuration of the system, artificial additional symmetry may be produced. BDI superconducting nanowire [36], discussed also in the chapter 4, is an example of such a case. The usual 2d class D Hamiltonian of a spin-orbit coupled material with external magnetic field in y direction reads [21]:

$$H = \left(\frac{p^2}{2m} - \mu\right)\tau_z + v_{so}(p_x \sigma_y \tau_z - p_y \sigma_x) + E_Z \sigma_x \tau_z + \Delta \sigma_y \tau_y, \tag{1.18}$$

where v_{so} is the scale, associated with the spin-orbit energy, and E_Z is the Zeeman energy due to magnetic field. The only symmetry of

the Hamiltonian is $\mathcal{P} = \tau_x K$, it belongs to class D. Notice, that if the transverse direction of a nanowire made from such a material is small compared to the spin-orbit length, then:

$$H' = \left(\frac{p^2}{2m} - \mu\right)\tau_z + v_{so} p_x \sigma_y \tau_z + E_Z \sigma_x \tau_z + \Delta \sigma_y \tau_y, \tag{1.19}$$

which has an additional symmetry $\mathcal{T} = K$ and brings the system into BDI symmetry class.

1.4 Effective theories of topological phase transitions

We now proceed to the description of the generic topological phase transition. Once the system is in symmetry class AIII, D, DIII, BDI or CII in 1 dimension, it can be made topological. Which means, under some parameters it will have end states. The transition to such state is always accompanied with the bulk gap closing. Actually, the mechanism of forming edge states is the same: the transition is in real space, with edge being the region of the closed gap on the boundary.

Near the transition the system can always be described by the linear dispersion with a small gap opening on either sides of it. Exactly at the transition the Hamiltonian reads:

$$p\sigma \otimes \tau, \tag{1.20}$$

where the subscript and the structure of the σ and τ matrices is chosen based on the symmetry class.

For the purposes of this thesis we will concentrate on the 1d case and derive the effective theories near the topological transition for all the classes. The symmetries in the topological classes are [10]: AIII – $\mathcal{C}$; BDI – $\mathcal{P}^2 = 1$, $\mathcal{T}^2 = 1$; DIII – $\mathcal{P}^2 = 1$, $\mathcal{T}^2 = -1$; D – $\mathcal{P}^2 = 1$; and CII – $\mathcal{P}^2 = -1$, $\mathcal{T}^2 = -1$. Let us describe the minimal models, tuning through the topological transition for all the classes above.

The most simple one is for the class D (also discussed later on in the chapter 3) and may be written in the basis of the states, for which the topological gap closes, as:

$$H_{\mathrm{D}} = v_0 p \sigma_0 + v_z p \sigma_z + a \sigma_y. \tag{1.21}$$

Here $v_z \pm v_0$ are the velocities of right (left) movers and a is the parameter, tuning through the topological transition, $a = 0$ is the point of

the transition. The only symmetry the Hamiltonian has is the particle-hole symmetry $\mathcal{P} = K$. There always is a Majorana bound state on the boundary between $a > 0$ and $a < 0$ regions.

By analogy, in the symmetry class AIII:

$$H_{\text{AIII}} = \mu\sigma_z + v_z p\sigma_z + a\sigma_y, \tag{1.22}$$

and the only symmetry here is the chiral one $\mathcal{C} = \sigma_x$, as all the anti-unitary symmetries act differently on $\mu\sigma_z$ and $p\sigma_z$. Again a tunes through the transition. The most well-known example of a system from the symmetry class is polyacetylene, which is described exactly by the model above. There the excitations on the boundary of the two phases are fermions with the charge which is half of an electron charge. Note that the AIII case and the D one have very similar phenomenology, since they coincide for $v_z = \mu = 0$.

Now, BDI is the version of class D with time-reversal symmetry, which squares to $+1$. Minimal model for that is:

$$H_{\text{BDI}} = v_z p\sigma_z + a\sigma_y, \tag{1.23}$$

where the symmetries read: $\mathcal{P} = K$, $\mathcal{T} = \sigma_x K$. The BDI class has $\mathbb{Z}$ topological number, but the model above describe the system only near one of the possible series of topological transitions. The excitations of the phase boundaries are multiple Majorana bound states, decoupled due to the time-reversal symmetry. The way to obtain this class in the nanowire setup was described above and we will return to it in the section 4.

We proceed with DIII case, where the minimal Hamiltonian must be written in a 4×4 matrix form, as at the transition point there are 4 states with nearly zero energy (particle-hole partners along with Kramers ones). Then:

$$H_{\text{DIII}} = v_{0z} p\tau_z + a\tau_z\sigma_y + b\tau_y + c\tau_y\sigma_z, \tag{1.24}$$

and $\mathcal{T} = \tau_x\sigma_y K$ and $\mathcal{P} = K$. The minimal number of terms in the minimal Hamiltonian is 4 for 4×4 one with both $\mathcal{T}$ and $\mathcal{P}$ symmetries. This can be understood as following: we need that there is no possible unitary symmetry on top of the two. That means that any combination of Pauli matrices should not commute with the Hamiltonian. For that you need at least $2 \times 2 = 4$ matrices, as one needs two in both Pauli matrix spaces. It is easy to see that if we put $b = c = 0$, the phase

boundary is at $a = 0$. Indeed, then there are two decoupled blocks of class D, where the transition is at $a = 0$. Once we couple them with b and c, we cannot remove the degeneracy between the Majorana modes, as they are Kramers pair of each other.

The last remaining class is CII, where:

$$H_{\mathrm{CII}} = v_{yz} p \sigma_y \tau_z + a \tau_y + b \sigma_x \tau_x + c \tau_z, \tag{1.25}$$

and the symmetries are $\mathcal{P} = \tau_y K$, $\mathcal{T} = \tau_z \sigma_y K$, again for $b = c = 0$ phase boundary is $a = 0$, as then the model is two decoupled AIII systems at that point. These subsystems are eigenfunctions of σ_y with eigenvalues ± 1, and the chiral symmetry $\mathcal{C} = \tau_x \sigma_y$ acts within a block.

1.5 Scattering matrix description

The Hamiltonians above can easily be transformed into scattering matrices of finite systems, described by these Hamiltonians. For any 1d system we can write a transfer matrix, connecting the right and the left ends of it. As all the Hamiltonians above are of the form $H = Ap + B$, where A and B are some matrices, the transfer matrix at energy ϵ is:

$$A \frac{\partial \psi}{\partial x} = (iB - i\epsilon)\psi, \tag{1.26}$$

$$\psi(x) = \exp\left[A^{-1}(iB - i\epsilon)x\right] \psi(0). \tag{1.27}$$

Transfer matrix M of a system of length L then reads:

$$M = \exp\left[A^{-1}(iB - i\epsilon)L\right]. \tag{1.28}$$

This matrix can be transformed into scattering matrix either from one side of a closed system (for that one finds the boundary conditions on the far end of the system, see chapter 3 for an example), or constructs a scattering matrix of a system, open from both sides by choosing the propagation basis on both sides. For the first approach we write the boundary condition on the far end of the wire of a general kind:

$$(1 - Q)\psi_{\mathrm{right}} = 0, \tag{1.29}$$

where Q is the hermitian unitary matrix, which has only eigenvalues $+1$ and -1, but it also must have equal number of them, $+1$ for the

wavefunctions (eigenfunctions of the matrix), growing in the direction outside the wire, and -1 for all other. Then we write the transfer matrix in the basis of in- and outgoing waves:

$$M \begin{pmatrix} \psi_{\text{in}} \\ \psi_{\text{out}} \end{pmatrix} = \psi_{\text{right}}, \tag{1.30}$$

$$(1-Q)M \begin{pmatrix} 0 \\ \psi_{\text{out}} \end{pmatrix} = (1-Q)M \begin{pmatrix} \psi_{\text{in}} \\ 0 \end{pmatrix} \tag{1.31}$$

The symmetries of the scattering matrix can be deduced from the procedure above, but a more simple way is to look at an infinitely narrow piece of the material in question. Then the scattering matrix coincides with the time evolution matrix over the time the particle takes to scatter. There are now time shifts in such a setup. Then:

$$S(\epsilon) = e^{i\Delta t(H-\epsilon)}, \tag{1.32}$$

and the symmetries of H are directly transformed into the ones of the S. For example:

$$KHK = -H, \tag{1.33}$$

$$KS(\epsilon)K = e^{i\Delta t(H+\epsilon)} = S(-\epsilon). \tag{1.34}$$

This symmetries transform into the analytical properties of the S. For example for the matrix above:

$$KS(\epsilon + i\Gamma)K = S(-\epsilon + i\Gamma). \tag{1.35}$$

This will be used in the chapter 2, where we will study the analytical properties of the scattering matrices in more details.

1.6 This thesis

1.6.1 Chapter 2

Motivated by the recent developments in the field of one-dimensional topological superconductors, in this chapter we investigate the topological properties of the scattering matrix of generic superconducting junctions where dimension should not play any role. We argue that for any finite junction the scattering matrix is always topologically trivial.

The apparent contradiction with the previous results is resolved by taking into account the low-energy resonant poles of the scattering matrix. Thus, no common topological transition occurs in a finite junction. This is what one expects from the general theory of phase transitions, which predicts that they become crossovers in finite systems. A transition of a different kind is revealed. It concerns the configuration of the resonant poles of the scattering matrix of the system. We also introduce a sample setup, where the transition can be artificially induced. In later chapters we will return to this transition.

1.6.2 Chapter 3

This chapter builds on the the results of the previous one and addresses the correspondence between the common topological transition in infinite system and the topological transition of the other type that manifests itself in the positions of the poles of the scattering matrices. The setup studied is a nanowire coupled to a lead through a tunnel barrier. In the vicinity of the common transition we establish a universal dependence of the pole positions on the parameter controlling the transition. The manifestations of the pole transitions in the differential conductance are discussed.

1.6.3 Chapter 4

This chapter shows that weak antilocalization by disorder competes with resonant Andreev reflection from a Majorana zero-mode and produces a zero-voltage conductance peak of order e^2/h in a superconducting nanowire. The phase conjugation needed for quantum interference to survive a disorder average is provided by particle-hole symmetry - in the absence of time-reversal symmetry and without requiring a topologically nontrivial phase. We identify methods to distinguish the Majorana resonance from the weak antilocalization effect. The mechanism for the individual system to show a peak in zero-bias conductance is the pole transition studied in chapters 2 and 3. An example of the dependence of the conductance of a single normal metal-superconductor contact is shown in fig. 1.6.

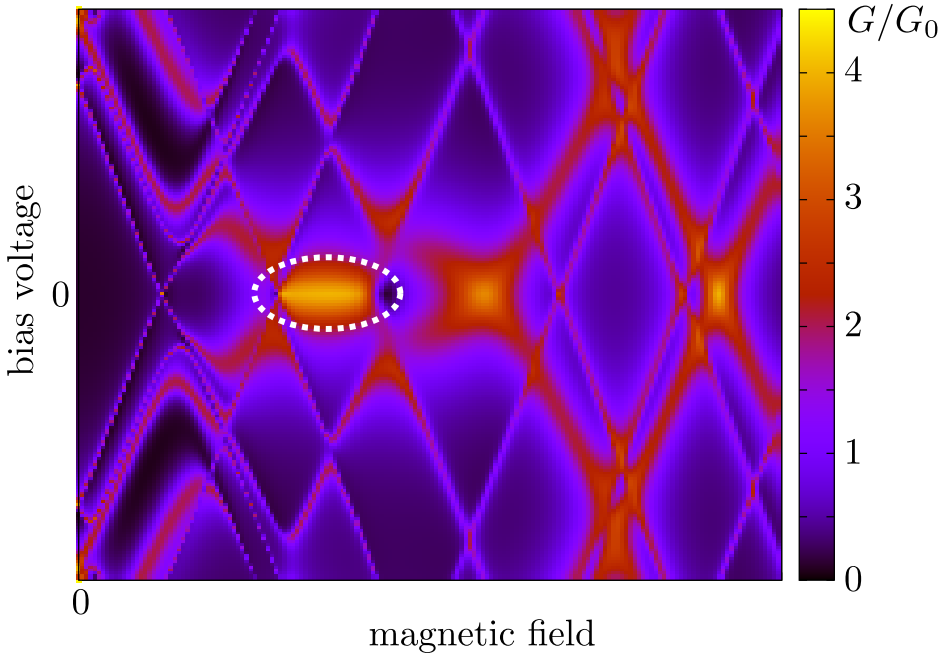

Figure 1.6. Example of a conductance dependence of magnetic field and bias voltage for a narrow nanowire. It shows that the zero-bias peak is developed in a region of magnetic fields, and the peak is not connected with the topology, but with the pole transition from chapters 2 and 3. Averaging over the systems gives the effect, discussed in the chapter 4, weak antilocalization.

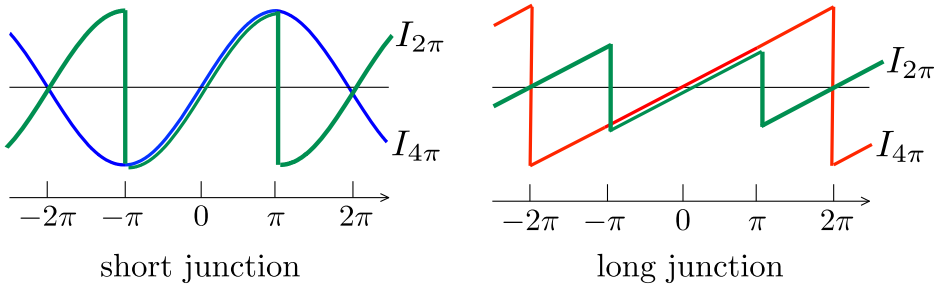

Figure 1.7. Sketch of the dependences of the 2π (parity non-conserving) and 4π (parity conserving) supercurrents for long and short Josephson junctions. The picture shows doubling of the supercurrent in the case of the long junction.

1.6.4 Chapter 5

In this chapter we study the other setup, already discussed in the chapter 2, Josephson junction made with a topological nanowire. We derive and discuss a generic phenomenological model that accounts for avoided crossing of Andreev states. This allows for a model-independent study. We investigate the dynamics of the junction at constant bias voltage to reveal an unexpected pattern of *any-*π Josephson effect in the limit of slow decoherence.

1.6.5 Chapter 6

This chapter investigates the Josephson current through the helical edge state of a quantum spin-Hall insulator. The separation L between the superconducting electrons and the coherence length ξ can have arbitrary relation with each other. We calculate the maximum (critical) current I_c that can flow without dissipation along a single edge, going beyond the short-junction restriction $L \ll \xi$ of earlier work, and find a dependence on the fermion parity of the ground state when L becomes larger than ξ. Fermion-parity conservation doubles the critical current in the low-temperature, long-junction limit, while for a short junction I_c is the same with or without parity constraints, see fig. 1.7. This provides a phase-insensitive, DC signature of the 4π-periodic Josephson effect.

1.6.6 Chapter 7

This chapter steps out of the main topic of the current thesis. Motivated by recent interest in the Nernst effect in cuprate superconductors, we calculate the magneto-thermo-electric effect for an arbitrary (anisotropic) quasiparticle dispersion relation and elastic scattering rate. The exact solution of the linearised Boltzmann equation is compared with the commonly used relaxation-time approximation. We find qualitative deficiencies of this approximation, to the extent that it can get the sign wrong of the Nernst coefficient. Ziman's improvement of the relaxation-time approximation, which becomes exact when the Fermi surface is isotropic, also cannot capture the combined effects of anisotropy in dispersion and scattering.

Bibliography

[1] K. von Klitzing, G. Dorda and M. Pepper, Phys. Rev. Lett. **45**, 494 (1980).

[2] C. L. Kane and E. J. Mele, Phys. Rev. Lett. **95**, 226801 (2005).

[3] B. A. Bernevig, T. L. Hughes, and S.-C. Zhang, Science, **314**, 1757 (2006).

[4] M. König, S. Wiedmann, C. Brüne, A. Roth, H. Buhmann, L. W. Molenkamp, X.-L. Qi, and S.-C. Zhang, Science **318**, 766 (2007).

[5] L. Fu, C. L. Kane and E. J. Mele, Phys. Rev. Lett. **98**, 106803 (2007).

[6] J. E. Moore and L. Balents, Phys. Rev. B **75**, 121306(R) (2007).

[7] D. Hsieh, D. Qian, L. Wray, Y. Xia, Y. S. Hor, R. J. Cava, and M. Z. Hasan, Nature **452**, 970 (2008).

[8] L. Fu and C. L. Kane, Phys. Rev. Lett. **100**, 096407 (2008).

[9] J. Nilsson, A. R. Akhmerov, and C. W. J. Beenakker, Phys. Rev. Lett. **101**, 120403 (2008).

[10] A. P. Schnyder, S. Ryu, A. Furusaki and A. W. W. Ludwig, Phys. Rev. B **78**, 195125 (2008).

[11] C. W. J. Beenakker, Annu. Rev. Con. Mat. Phys. **4**, 113 (2013).

[12] J. Alicea, Rep. Prog. Phys. **75**, 076501 (2012).

[13] G. Moore and N. Read, Nucl. Phys. B **360** 362 (1991).

[14] D. A. Ivanov, Phys. Rev. Lett. **86**, 268 (2001).

[15] A. Yu. Kitaev Phys. Usp. **44**, 131 (2001).

[16] A. Yu. Kitaev Ann. Phys. **303**, 2 (2013).

[17] J. Alicea, Y. Oreg, G. Refael, F. von Oppen, and M. P. A. Fisher, Nature Physics **7**, 412 (2011).

[18] T. Hyart, B. van Heck, I. C. Fulga, M. Burrello, A. R. Akhmerov, and C. W. J. Beenakker, Phys. Rev. B **88**, 035121 (2013).

[19] C. Nayak, S. H. Simon, A. Stern, M. Freedman, and S. Das Sarma, Rev. Mod. Phys. **80**, 1083 (2008).

[20] L. Fu and C. L. Kane, Phys. Rev. B **79**, 161408R (2009).

[21] R. M. Lutchyn, J. D. Sau, and S. Das Sarma, Phys. Rev. Lett. **105**, 077001 (2010).

[22] Y. Oreg, G. Refael, and F. von Oppen, Phys. Rev. Lett. **105**, 177002 (2010).

[23] V. Mourik, K. Zuo, S. M. Frolov, S. R. Plissard, E. P. A. M. Bakkers, and L. P. Kouwenhoven, Science **336**, 1003 (2012).

[24] M. T. Deng, C. L. Yu, G. Y. Huang, M. Larsson, P. Caroff, and H. Q. Xu, Nano Lett. **12**, 6414-6419 (2012).

[25] A. Das, Y. Ronen, Y. Most, Y. Oreg, M. Heiblum, and H. Shtrikman, Nature Physics **8**, 887 (2012).

[26] L. P. Rokhinson, X. Liu, and J. K. Furdyna, Nature Physics **8**, 795 (2012).

[27] A. F. Andreev, Sov. Phys. JETP **19**, 1228 (1964).

[28] Shuo Mi, D. I. Pikulin, M. Wimmer, and C. W. J. Beenakker, Phys. Rev. B **87**, 241405(R) (2013).

[29] K. T. Law, P. A. Lee, and T. K. Ng, Phys. Rev. Lett. **103**, 237001 (2009).

[30] C. W. J. Beenakker, Rev. Mod. Phys. **69**, 731 (1997).

[31] Y. V. Nazarov and Y. M. Blanter, *Quantum Transport*, (Cambridge University Press, Cambridge, 2009).

[32] B. D. Josephson, Rev. Mod. Phys. **36**, 216 (1964).

[33] P.-G. de Gennes, *Superconductivity of Metals and Alloys*, Addison-Wesley, Reading, MA (1986).

[34] L. Fu, Phys. Rev. Lett., **106**, 106802 (2011).

[35] I. C. Fulga, F. Hassler, and A. R. Akhmerov, Phys. Rev. B **85**, 165409 (2012).

[36] S. Tewari and J. D. Sau, Phys. Rev. Lett. **109**, 150408 (2012).